Meccanica (2012) 47:1173–1184
DOI 10.1007/s11012-011-9502-5

Heat and mass transfer by MHD mixed convection stagnation point flow toward a vertical plate embedded in a highly porous medium with radiation and internal heat generation

O.D. Makinde

Received: 30 January 2011 / Accepted: 13 October 2011 / Published online: 8 November 2011

Abstract This paper examined the hydromagnetic mixed convection stagnation point flow towards a vertical plate embedded in a highly porous medium with radiation and internal heat generation. The governing boundary layer equations are formulated and transformed into a set of ordinary differential equations using a local similarity approach and then solved numerically by shooting iteration technique together with Runge-Kutta sixth-order integration scheme. A representative set of numerical results are displayed graphically and discussed quantitatively to show some interesting aspects of the pertinent parameters on the dimensionless axial velocity, temperature and the concentration profiles, local skin friction, local Nusselt number and local Sherwood number, the rate of heat and mass transfer. Good agreement is found between the numerical results of the present paper with the earlier published works under some special cases.

Keywords Internal heat generation · Highly porous medium · Heat and mass transfer · Thermal radiation · Stagnation point flow · Mixed convection

O.D. Makinde (✉)
Institute for Advance Research in Mathematical Modelling and Computations, Cape Peninsula University of Technology, PO Box 1906, Bellville 7535, South Africa
e-mail: makinded@cput.ac.za

Nomenclature

g	gravitational acceleration
G_T	thermal Grashof number
(x, y)	Cartesian coordinates
C_w	plate surface concentration
C_∞	free stream concentration
C	fluid chemical species concentration
D	diffusion coefficient
f	dimensionless stream function
Nu	Nusselt number
T_∞	free stream temperature
$\tilde{K}$	porous media permeability
G_c	solutal Grashof number
Sh	Sherwood number
K	permeability parameter
T	fluid temperature
Pr	Prandtl number
T_w	plate surface temperature
S	heat generation/absorption parameter
k	thermal conductivity coefficient
Sc	Schmidt number
(u, v)	velocity components
Q	volumentric heat generation/absorption rate
K'	mean absorption coefficient
Ra	thermal radiation parameter
B_0	magnetic field of constant strength

Greek Letters

β^*	coefficient of expansion with concentration
β	coefficient of thermal expansion
μ	coefficient of viscosity

ρ density of fluid
ϕ dimensionless concentration
θ dimensionless temperature
η dimensionless variable
υ kinematic viscosity
Ψ stream function
σ^* Stefan-Boltzmann constant
σ_e fluid electrical conductivity

1 Introduction

Hydromagnetic mixed convection flows past a surface embedded in a saturated porous medium have received considerable attention because of numerous applications in engineering and geophysics [1]. Moreover, mixed convection flow of an electrically conducting fluid over a flat surface in the presence of a magnetic field is also of special technical significance because of its frequent occurrence in many industrial applications such as cooling of nuclear reactors, MHD marine propulsion, electronic packages, micro electronic devices etc. Some other quite promising applications are in the field of metallurgy such as MHD stirring of molten metal and magnetic-levitation casting. The analysis of hydromagnetic flows in porous media has been the subject of several recent papers [2–4]. Most of the published papers on convection in porous media under the action of a magnetic field deal with external flows, however, stagnation points do exist at the surface of objects in the flow field, where the fluid is brought to rest by the object. Considerable attention has been given to the study of 2-D stagnation point flow [5–10]. Hiemenz [11] derived an exact solution of the steady flow of a Newtonian fluid impinging orthogonally on an infinite plane. Singh et al. [12] studied the effect of volumentric heat generation/absorption on mixed convection stagnation point flow on an isothermal vertical plate in porous media.

Meanwhile, the radiative flow of an electrically conducting fluid arises in many practical applications such as in electrical power generation, astrophysical flows, solar power technology and nuclear reactors. Also, radiative heat mass transfer occurs in many geothermal, geophysical, technological and engineering applications. Thermal radiation is a characteristic of any flow system at temperatures above the absolute zero and can strongly interact with convection in many situations of engineering interest. The effects of radiation on the boundary layer flow with and without a magnetic field under different situations were studied by many investigators [13]. Chamkha et al. [14] analyzed the effect of radiation heat transfer on flow and thermal field in the presence of magnetic field for horizontal and inclined plates. The effect of thermal radiation on the heat and mass transfer flow of a variable viscosity fluid past a vertical porous plate permeated by a transverse magnetic field was reported by Makinde and Ogulu [15]. The hydromagnetic flow in the presence of radiation has been investigated by Bestman and Adiepong [16], Naroua et al. [17] and Ouaf [18] when the induced magnetic field is negligible. Raptis et al. [19] investigated the effects of radiation in an optically thin gray gas past a vertical infinite plate in the presence of a magnetic field, when the magnetic Reynolds number is not negligible and the flow is steady. The effect of thermal radiation in the linearized Rosseland approximation on the heat transfer characteristics of various boundary layer flows was reported by Magyari and Pantokratoras [20].

Our objective in this present study is to extend the recent work of Singh et al. [12] to include hydromagnetic mixed convection stagnation point flow with thermal radiation past a vertical plate embedded in a porous media. The governing boundary-layer equations have been transformed to a two-point boundary value problem using a local similarity approach, and these have been solved numerically. The effects of various embedded parameters on fluid velocity, temperature and concentration have been shown graphically. It is hoped that the results obtained will not only provide useful information for applications, but also serve as a complement to the previous studies.

2 Mathematical model

Consider steady laminar stagnation point flow of a viscous incompressible electrically conducting fluid through a porous medium along a vertical isothermal plate in the presence of volumentric rate of heat generation and magnetic field. It is assumed that the fluid property variations due to temperature and chemical species concentration are limited to fluid density. In addition, there is no applied electric field and all of the Hall effects and Joule heating are neglected. Since the magnetic Reynolds number is very small for most fluid used in industrial applications, we assume that the induced magnetic field is negligible. The x-axis is taken

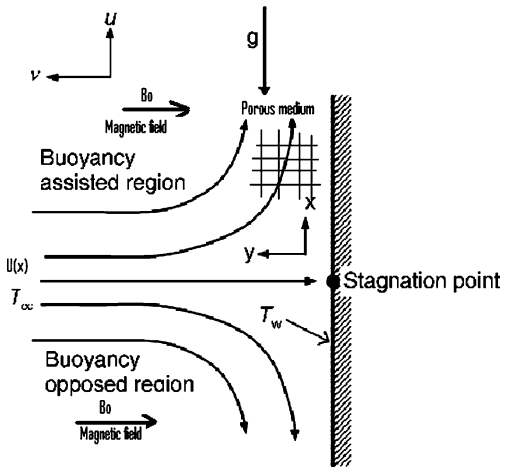

Fig. 1 Schematic diagram of the problem

along the plate and y-axis is normal to the plate and the flow is confined in half plane $y > 0$ as shown in Fig. 1. The potential flow arrives from the y-axis and impinges on plate, which divides at stagnation point into two streams and the viscous flow adheres to the plate. The velocity distribution in the potential flow is given by $U_\infty = cx$, where c is a positive constant.

Following [5–10] the linear Darcy term representing distributed body force due to porous media is retained while the non-linear Forchheimer term is neglected, thus the governing equations of continuity, momentum, energy and species concentration are given by

$$\frac{\partial u}{\partial x} + \frac{\partial v}{\partial y} = 0, \tag{1}$$

$$u\frac{\partial u}{\partial x} + v\frac{\partial u}{\partial y} = \upsilon\frac{\partial^2 u}{\partial y^2} + g\beta(T - T_\infty) + g\beta^*(C - C_\infty) - \left(\frac{\sigma_e B_0^2}{\rho} + \frac{\upsilon}{\tilde{K}}\right)(u - U_\infty) + U_\infty\frac{dU_\infty}{dx}, \tag{2}$$

$$u\frac{\partial T}{\partial x} + v\frac{\partial T}{\partial y} = \alpha\frac{\partial^2 T}{\partial y^2} - \frac{\alpha}{k}\frac{\partial q_r}{\partial y} + Q(C - C_\infty), \tag{3}$$

$$u\frac{\partial C}{\partial x} + v\frac{\partial C}{\partial y} = D\frac{\partial^2 C}{\partial y^2}. \tag{4}$$

The boundary conditions are

$$\begin{aligned} &u = 0, \quad v = 0, \quad T = T_w, \quad C = C_w \\ &\quad \text{at } y = 0, \\ &u \to U_\infty = cx, \quad T \to T_\infty, \quad C \to C_\infty \\ &\quad \text{as } y \to \infty, \end{aligned} \tag{5}$$

where u and v are the velocity components in the x- and y-directions, respectively, ρ is the fluid density, υ is the kinematic viscosity, σ_e is the electrical conductivity of the fluid, $\tilde{K}$ is the permeability of the porous medium, g is the gravitational acceleration, β is the thermal expansion coefficient, β^* is the coefficient of expansion with concentration, T is the temperature, c_p is the specific heat capacity at constant pressure of the fluid, α is the thermal diffusivity of the fluid, k is thermal conductivity, T_w is the temperature of the plate, Q is the volumentric rate heat generation, B_0 is the magnetic field of constant strength and D is the coefficient of mass diffusivity. Using the Rosseland approximation, the radiative heat flux in the y-direction is given by Sparrow and Cess [13],

$$q_r = -\frac{4\sigma^*}{3K'}\frac{\partial T^4}{\partial y}, \tag{6}$$

where σ^* and K' are the Stefan-Boltzmann constant and the mean absorption coefficient, respectively. As done by Makinde and Ogulu [15], temperature differences within the flow are assumed to be sufficiently small so that T^4 may be expressed as a linear function of temperature T using a truncated Taylor series about the free stream temperature T i.e.

$$T^4 \approx 4T_\infty^3 T - 3T_\infty^4. \tag{7}$$

We introduce the following non-dimensional variables:

$$\begin{aligned} &\eta = y\sqrt{\frac{c}{\upsilon}}, \qquad \psi(x, y) = \sqrt{\upsilon c}xf(\eta), \\ &\theta(\eta) = \frac{T - T_\infty}{T_w - T_\infty}, \qquad \phi(\eta) = \frac{C - C_\infty}{C_w - C_\infty}, \\ &G_T = \frac{g\beta(T_w - T_\infty)x^3}{\upsilon^2}, \qquad G_c = \frac{g\beta(C_w - C_\infty)x^3}{\upsilon^2}, \\ &Ra = \frac{4\sigma^* T_\infty^3}{kK'}, \qquad \mathrm{Re}_x = \frac{U_\infty x}{\upsilon}, \\ &K = \frac{\upsilon}{c\tilde{K}}, \qquad Pr = \frac{\upsilon}{\alpha}, \qquad Sc = \frac{\upsilon}{D}, \\ &\upsilon = \frac{\mu}{\rho}, \qquad M = \frac{\sigma_e B_0^2}{c\rho}, \qquad S = \frac{Q(C_w - C_\infty)\upsilon}{c\alpha(T_w - T_\infty)}, \end{aligned} \tag{8}$$

where ψ is the stream function which is defined in the usual form as $u = \partial\psi/\partial x$ and $v = -\partial\psi/\partial y$ so

that the continuity equation (1) is automatically satisfied. Substituting the expression in (7) together with the similarity variables in (8) into (1)–(5), we obtain the following nonlinear ordinary differential equations:

$$f''' + ff'' - f'^2 + G_T\theta + G_c\phi - (K+M)(f'-1) + 1 = 0, \tag{9}$$

$$\left(1 + \frac{4}{3}Ra\right)\theta'' + Pr\, f\theta' + S\phi = 0, \tag{10}$$

$$\phi'' + Sc\, f\phi' = 0, \tag{11}$$

where K is the porous medium permeability parameter, Ra is the thermal radiation parameter, G_T is the local thermal Grashof number, G_c is the local solutal Grashof number, Pr is the Prandtl number, Sc is the Schmidt number, M is the magnetic field intensity parameter and S is the internal heat generation parameter. The corresponding boundary conditions (5) now becomes

$$\begin{aligned} &f = 0, \quad f' = 0, \quad \theta = 1, \quad \phi = 1 \quad \text{at } \eta = 0, \\ &f' = 1, \quad \theta = 0, \quad \phi = 0 \quad \text{as } \eta \to \infty. \end{aligned} \tag{12}$$

The set of (9)–(11) under the boundary conditions (12) have been solved numerically by applying the Nachtsheim and Swigert [21] shooting iteration technique together with Runge-Kutta sixth-order integration scheme. From the process of numerical computation, the skin-friction coefficient, the local Nusselt number and the local Sherwood number, which are respectively given by

$$C_f = \frac{2\tau_w}{\rho U_\infty^2}, \qquad Nu = \frac{xq_w}{k(T_w - T_\infty)}, \qquad Sh = \frac{xq_m}{D(C_w - C_\infty)}, \tag{13}$$

where

$$\tau_w = \mu \left.\frac{\partial u}{\partial y}\right|_{y=0}, \qquad q_w = -k \left.\frac{\partial T}{\partial y}\right|_{y=0} - \left.\frac{4\sigma^*}{3K'}\frac{\partial T^4}{\partial y}\right|_{y=0}, \qquad q_m = -D \left.\frac{\partial C}{\partial y}\right|_{y=0}. \tag{14}$$

Substituting (7), (8) and (15) into (14), we obtained the expressions for the skin-friction coefficient, the local Nusselt number and the local Sherwood number as

$$\begin{aligned} &\mathrm{Re}_x^{1/2} C_f = f''(0), \\ &\mathrm{Re}_x^{-1/2} Nu = -(1 + 4Ra/3)\theta'(0), \\ &\mathrm{Re}_x^{-1/2} Sh = -\phi'(0). \end{aligned} \tag{15}$$

The accuracy of our numerical procedure is tested by direct comparisons with the previously published work of Singh et al. [12] for special cases of the problem under consideration. Table 1 shows that excellent agreement between the compared results exists. This lends confidence in the numerical results to be reported subsequently.

3 Results and discussions

In order to get a clear insight on the physics of the problem, a parametric study is performed and the obtained numerical results are displayed with the help of graphical illustrations. We focus on the positive values of the buoyancy parameters i.e. Grashof number $G_T > 0$ (which corresponds to the cooling problem) and solutal Grashof number $G_C > 0$ (which indicates that the chemical species concentration in the free stream region is less than the concentration at the boundary surface). The cooling problem is of-

Table 1 Computations showing the comparison with Singh et al. [12] for different values of S when $G_T = 1.0$, $G_c = 0.5$, $Pr = 1$, $Sc = 0.5$, $M = 0$, $Ra = K = 0$

S	$f''(0)$ [12]	$-\theta'(0)$ [12]	$-\phi'(0)$ [12]	$f''(0)$ Present	$-\theta'(0)$ Present	$-\phi'(0)$ Present
−1	1.8444	1.3908	0.4631	1.844462	1.390856	0.463174
0	1.9995	0.6392	0.4789	1.999553	0.639244	0.478964
1	2.1342	−0.0730	0.4917	2.134287	−0.073040	0.491749

Table 2 Computations showing $f''(0)$, $-\theta'(0)$, $-\phi'(0)$ for various values of embedded parameters

S	K	Pr	G_T	G_C	Sc	M	Ra	$f''(0)$	$-\theta'(0)$	$-\phi'(0)$
0	1	0.1	1	0.5	0.5	0.1	0.1	2.389898	0.236593	0.502813
0.5	1	0.1	1	0.5	0.5	0.1	0.1	2.477113	−0.20393	0.513073
1	3	0.1	1	0.5	0.5	0.1	0.1	2.878166	−0.64378	0.518639
1	5	0.1	1	0.5	0.5	0.1	0.1	3.184808	−0.65098	0.517897
1	1	1	1	0.5	0.5	0.1	0.1	2.370055	−0.04316	0.494804
1	1	10	1	0.5	0.5	0.1	0.1	2.154799	1.073118	0.474395
1	1	0.1	0.5	0.5	0.5	0.1	0.1	2.220679	−0.68158	0.496618
1	1	0.1	0.7	0.5	0.5	0.1	0.1	2.358558	−0.65897	0.507416
1	1	0.1	0.5	1	0.5	0.1	0.1	2.437256	−0.66294	0.507347
1	1	0.1	0.5	2	0.5	0.1	0.1	2.856783	−0.63004	0.526974
1	1	0.1	0.5	0.5	1	0.1	0.1	2.170082	−0.49096	0.653140
1	1	0.1	0.5	0.5	2	0.1	0.1	2.125898	−0.33929	0.851850
1	1	0.1	0.5	0.5	0.5	1	0.1	2.305895	−0.05390	0.859057
1	1	0.1	0.5	0.5	0.5	3	0.1	2.704379	−0.04824	0.879438
1	1	0.1	0.5	0.5	0.5	0.1	1	2.103755	0.006342	0.848097
1	1	0.1	0.5	0.5	0.5	0.1	3	2.104745	0.049987	0.848680

ten encountered in engineering applications. The values of Schmidt number (Sc) were chosen to be $Sc = 0.24, 0.62, 0.78, 2.62$, representing diffusing chemical species of most common interest in air like H_2, H_2O, NH_3, and Propyl Benzene respectively while the values of Prandtl number ranges $Pr = 0.72$ (Air) to 7.1 (water). From Table 2, it is interesting to note that the local skin friction at the plate surface increases with increasing parameter values of M, S, G_T, G_c, Ra and K and decreases with increasing values of Prandtl number and Schmidt number. This implies that combined effect of buoyancy forces, magnetic field, thermal radiation, internal heat generation and decreasing porous medium permeability is to increase the local skin friction at the plate surface. Similarly, the local Nusselt number (Nu) coefficient at the plate surface increases with an increase in parameter values of G_T, G_c, M, K, and Pr and decreases with an increase in S and Sc. Moreover, it is noteworthy that local Sherwood number (Sh) at the plate surface increases with a combined increase in the internal heat generated in the flow system ($S > 0$) and magnetic intensity ($M > 0$) and decreases with other parameters.

3.1 Effects of parameter variation on velocity profiles

Figures 2–8 depict the effects of emerging flow parameters on non-dimensional velocity profiles. Generally,

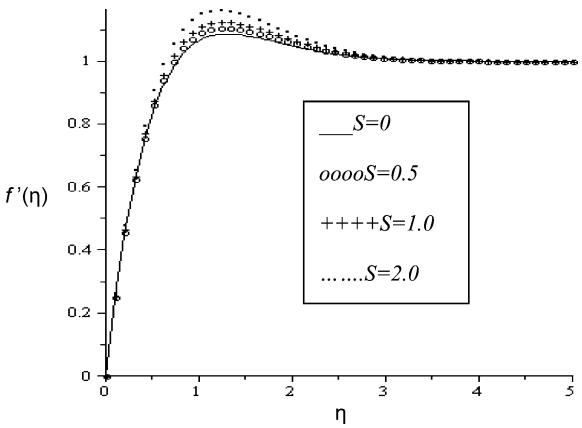

Fig. 2 Velocity profiles for $G_T = G_c = K = M = 1$, $Pr = 0.72$, $Sc = 0.62$, $Ra = 0.1$

the fluid velocity increases gradually from the stationary plate surface to its peak value within the boundary layer region, then converging to its free stream value far away from the plate satisfying the boundary condition. In Fig. 2 the effect of increasing the internal heat generation parameter on the velocity profiles is illustrated. It is noteworthy that an overshoot in the fluid velocity towards the plate surface is observed, consequently the peak value of the fluid velocity increases with an increase in the internal heat generation parameter (S). This can be attributed to the fact that increase

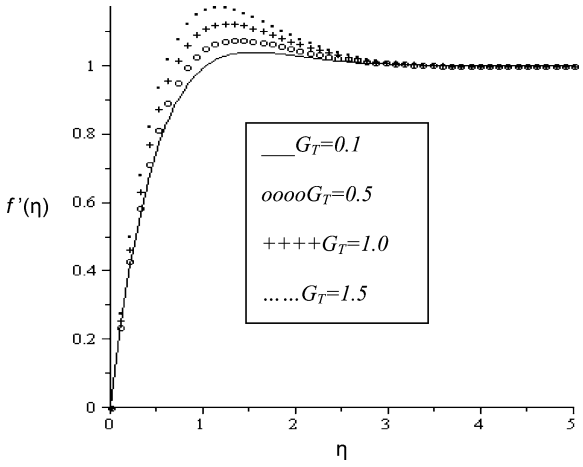

Fig. 3 Velocity profiles for $G_c = K = S = M = 1$, $Sc = 0.62$, $Pr = 0.72$, $Ra = 0.1$

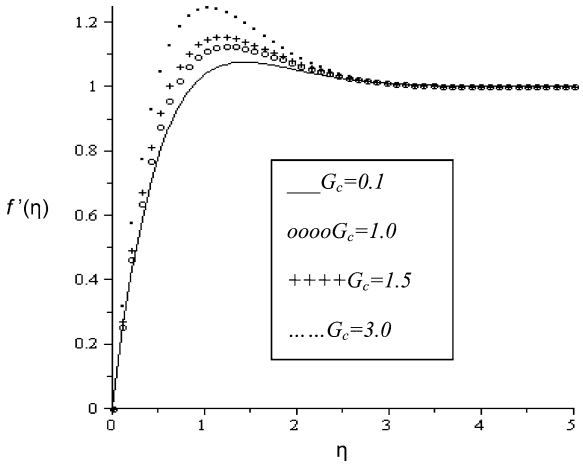

Fig. 4 Velocity profiles for $G_T = K = S = M = 1$, $Sc = 0.62$, $Pr = 0.72$, $Ra = 0.1$

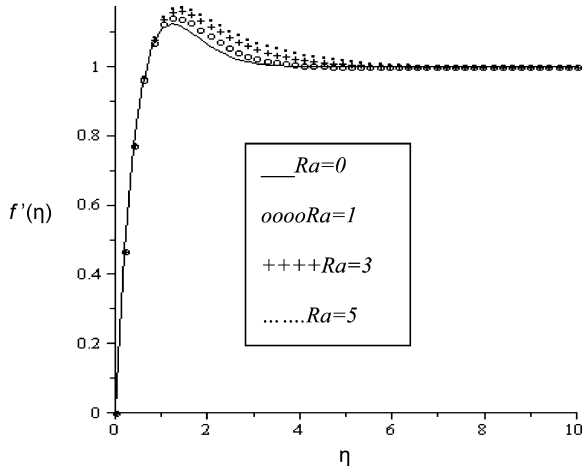

Fig. 5 Velocity profiles for $G_T = G_c = K = S = M = 1$, $Pr = 0.72$, $Sc = 0.62$

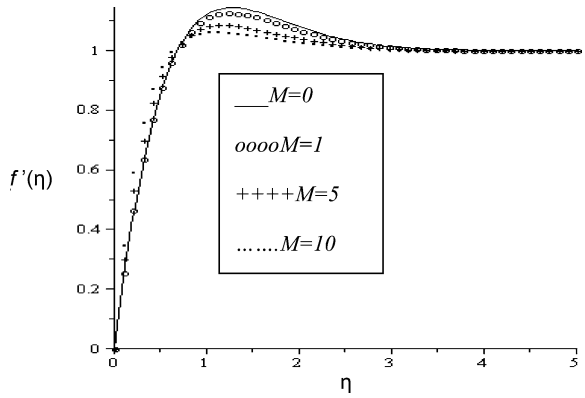

Fig. 6 Velocity profiles for $G_T = G_c = K = S = 1$, $Pr = 0.72$, $Sc = 0.62$, $Ra = 0.1$

in internal heat generation has the tendency to increase the fluid temperature which in turn causes an increased fluid velocity along the plate due to buoyancy effect. Similar trend is observed in Figs. 3–5 with increasing parameter values of G_T, G_c, and Ra. The fluid motion is enhanced by buoyancy forces with increasing values of thermal and solutal Grashof (Gr_x, Gc_x) leading to velocity overshoot towards the plate surface as the peak value of fluid velocity increases within the boundary layer. Thermal radiation also leads to increased acceleration of the fluid motion near the plate surface in the presence of buoyancy forces as shows in Fig. 5. Figure 6 depicts the influence of magnetic field parameter (M) on the velocity field. It is seen from this figure that the peak value of the velocity profiles decreases with increasing magnetic field intensity. Moreover, the effects of a transverse magnetic field on an electrically conducting fluid gives rise to a resistive-type force called the Lorentz force. This force has the tendency to slow down the fluid motion. This result qualitatively agrees with the expectations (Chamkha and Quadri [3]). From (9) it is expected that an increase in the parameter value of K (representing a decrease in the porous medium permeability) will produce the same effect on the fluid velocity profile i.e. by decreasing the value of peak velocity near the plate surface. Meanwhile, it is interesting to note that a decrease in the peak value of fluid velocity within the boundary layer is observed in Figs. 7 and 8 with an increase in Schmidt number (Sc) and Prandtl

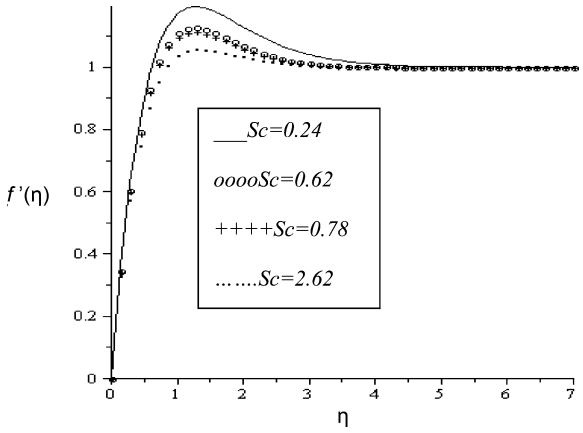

Fig. 7 Velocity profiles for $G_T = G_c = K = S = M = 1$, $Pr = 0.72$, $Ra = 0.1$

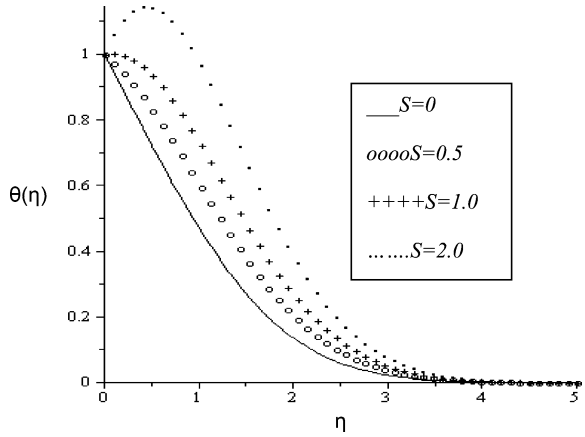

Fig. 9 Temperature profiles for $G_T = G_c = K = M = 1$, $Pr = 0.72$, $Sc = 0.62$, $Ra = 0.1$

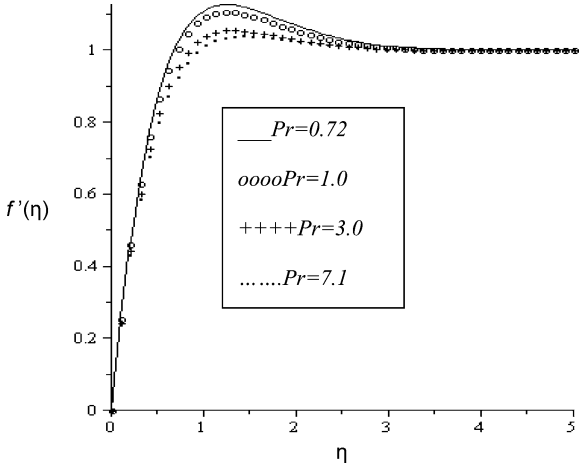

Fig. 8 Velocity profiles for $G_T = G_c = K = S = M = 1$, $Sc = 0.62$, $Ra = 0.1$

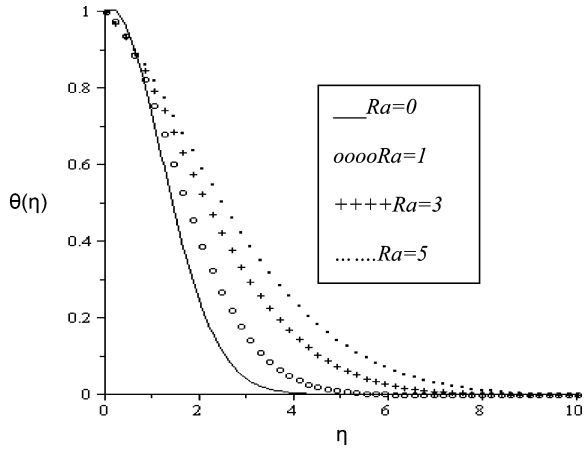

Fig. 10 Temperature profiles for $G_T = G_c = K = S = M = 1$, $Pr = 0.72$, $Sc = 0.62$

number (Pr). The physics behind this observation is that the increased Schmidt number and Prandtl number decreases chemical species molecular diffusivity and fluid thermal diffusivity, which ultimately reduces the velocity.

3.2 Effects of parameter variation on temperature profiles

Figures 9–14 illustrate the temperature field against spanwise coordinate η. The fluid temperature is highest at the plate surface and decreases exponentially to the free stream zero value far away from the plate satisfying the boundary condition. In Fig. 9, we observed an overshoot in the fluid temperature near the plate surface with increasing value of internal heat generation parameter. As more heat is generated within the fluid, the fluid temperature increases leading to steep temperature gradient between the plate surface and the fluid. The thermal boundary layer thickness also increases with an increase in internal heat generation in the flow field. An increase in the thermal radiation (Ra) causes an increase in the fluid temperature within the boundary layer and consequently the thermal boundary layer increases as shown in Fig. 10. Figures 11 and 12 depict the influence of Schmidt number and Prandtl number on the thermal boundary layer. It is seen that increase in Pr brings a decrease in the thermal boundary layer thickness. At high Prandtl number, the fluid velocity decreases, which in

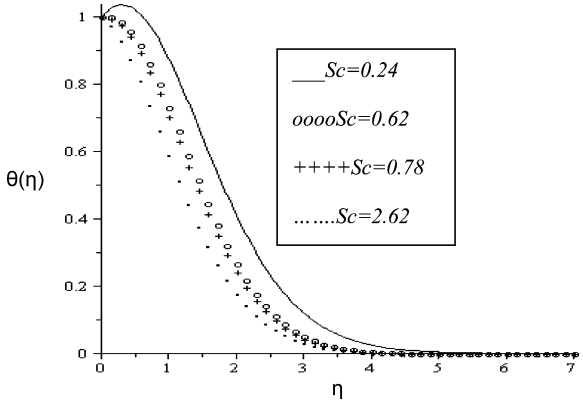

Fig. 11 Temperature profiles for $G_T = G_c = K = S = M = 1$, $Pr = 0.72$, $Ra = 0.1$

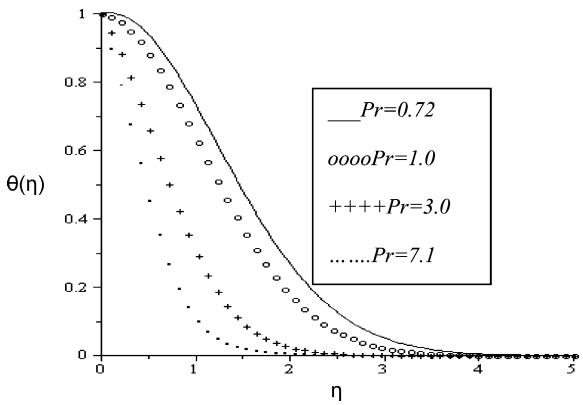

Fig. 12 Temperature profiles for $G_T = G_c = K = S = M = 1$, $Sc = 0.62$, $Ra = 0.1$

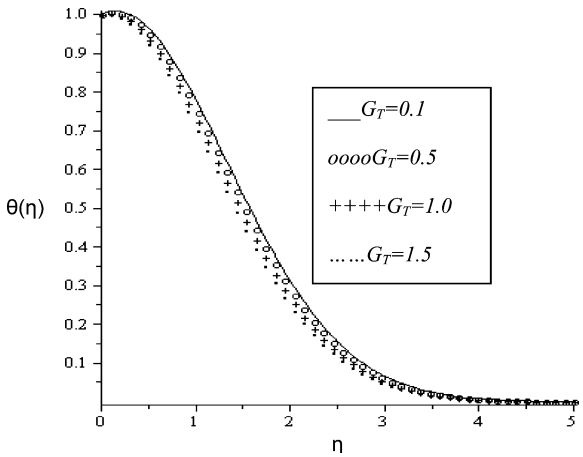

Fig. 13 Temperature profiles for $G_c = K = S = M = 1$, $Sc = 0.62$, $Pr = 0.72$, $Ra = 0.1$

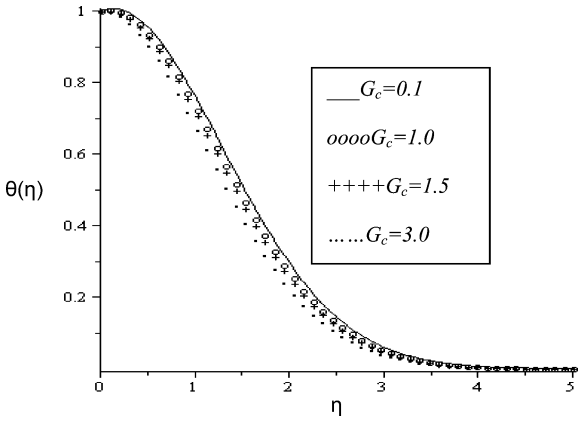

Fig. 14 Temperature profiles for $G_T = K = S = M = 1$, $Sc = 0.62$, $Pr = 0.72$, $Ra = 0.1$

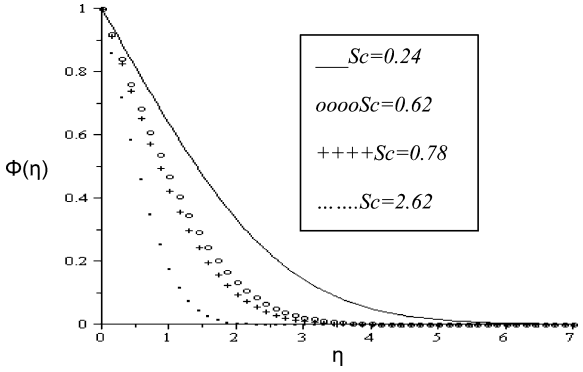

Fig. 15 Concentration profiles for $G_T = G_c = K = S = M = 1$, $Pr = 0.72$, $Ra = 0.1$

turn implies lower thermal diffusivity leading to a decrease in the fluid temperature. Similarly, as Schmidt number increases the thermal boundary layer thickness decreases due to a decrease in chemical species molecular diffusivity. In Figs. 13 and 14, it is observed that an increase in solutal Grashof number and thermal Grashof number cause a decrease in the thermal boundary layer thickness, and consequently the fluid temperature decreases due to buoyancy effect.

3.3 Effects of parameter variation on concentration profiles

Figures 15 and 16 illustrate the concentration profiles. The chemical species concentration is highest at the plate surface and decreases exponentially to

the free stream zero value far away from the plate. It is observed in Fig. 15 that an increase in Schmidt number (Sc) decreases the concentration boundary layer and this is analogous to the effect of increasing the Prandtl number on the thickness of a thermal boundary layer. A slight decrease in the concentration boundary layer is observed with an increase in solutal Grashof number due to buoyancy effect as depicted in Fig. 16.

3.4 Local skin friction, local nusselt number and local sherwood number

Figures 17–19 depict the influence of parameter variation on the local skin friction, local Nusselt number and local Sherwood number at the plate surface.

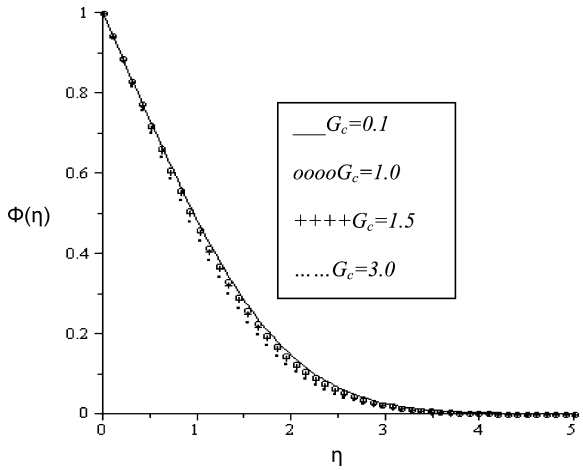

Fig. 16 Concentration profiles for $G_T = K = S = M = 1$, $Sc = 0.62$, $Pr = 0.72$, $Ra = 0.1$

The results highlighted in the figures are in agreement with the one reported in Table 2 above. It can be seen from Fig. 17 that the coefficient of skin friction increases with an increase in the internal heat generated in the fluid. As the Schmidt number (Sc) increases, local skin friction decreases due to a decrease in the velocity gradient at the plate surface. Moreover, an increase in the value of local skin friction is observed in Fig. 18 with increasing value of magnetic field parameter (M). Increase in the buoyancy effect due to temperature gradient causes a decrease in the local skin friction. In Fig. 19 it is interesting to note that at a very low Prandtl number, the plate surface is heated up by the fluid as internal heat generation within the fluid increases (i.e. the heat is transfer from the fluid to the plate). However, as the Prandtl number increases, the local Nusselt number increases. An increase in internal heat generation causes a general decrease in the local Nusselt number increases at the plate surface. Figure 20 shows that the rate of heat transfer at the plate surface increases with an increase in the parameter value of thermal radiation. This can be attributed to the fact that as thermal radiation increases, the dominance effect of temperature gradient increases, leading to an increase in the local Nusselt number. In Fig. 21, it is observed that the local Sherwood number increases with increasing value of Schmidt number due to a decrease in the chemical species molecular diffusivity and an increase in the concentration gradient at the plate surface. As the magnetic field intensity increases, a further increase in the local Sherwood number is observed.

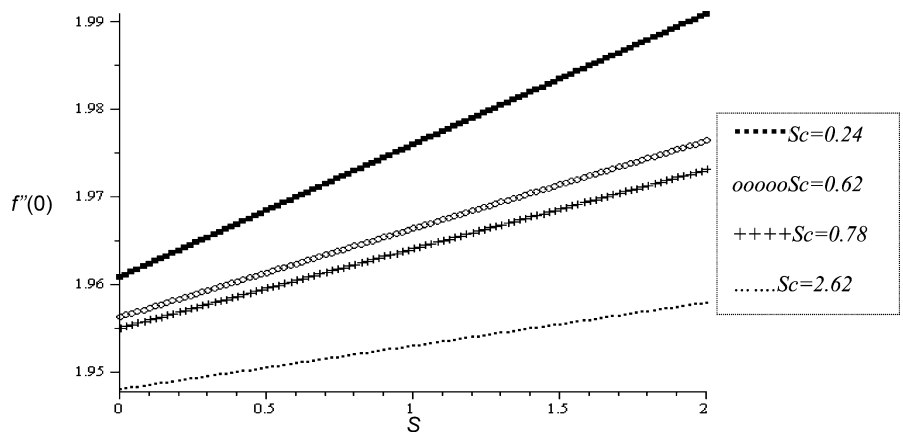

Fig. 17 Local skin friction for $G_T = G_c = Ra = 0.1$, $K = M = 1$, $Pr = 0.72$

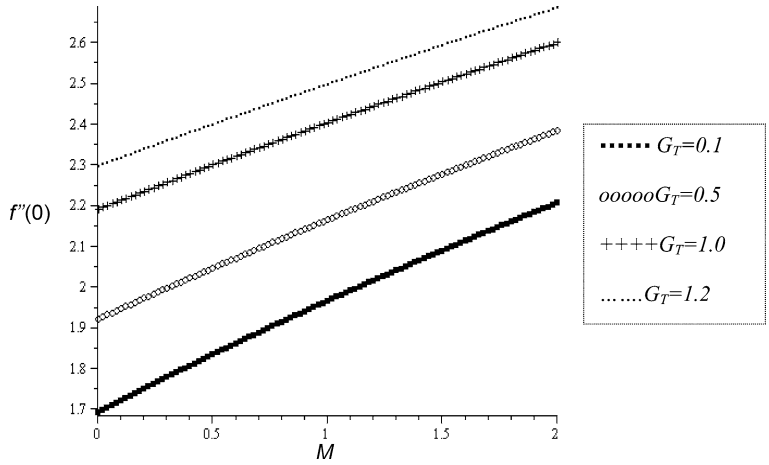

Fig. 18 Local skin friction for $G_c = Ra = 0.1$, $K = S = 1$, $Sc = 0.6$, $Pr = 0.72$

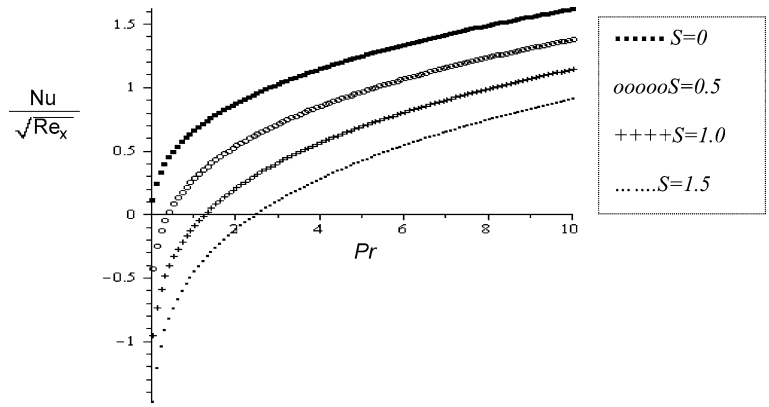

Fig. 19 Local Nusselt number for $G_c = G_T = Ra = 0.1$, $K = M = 1$, $Sc = 0.62$

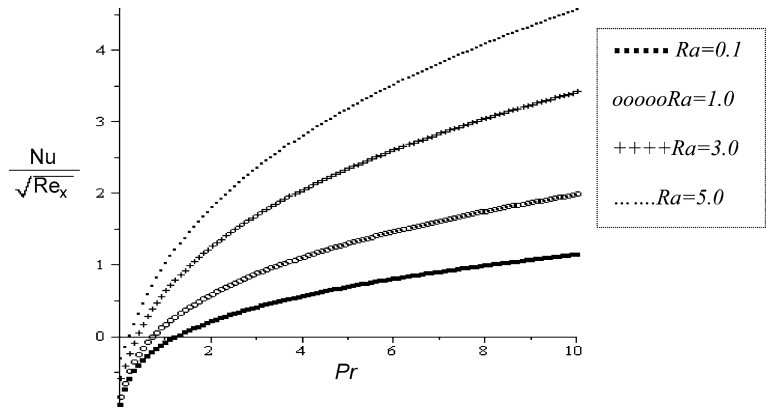

Fig. 20 Local Nusselt number for $G_c = G_T = 0.1$, $K = S = M = 1$, $Sc = 0.62$

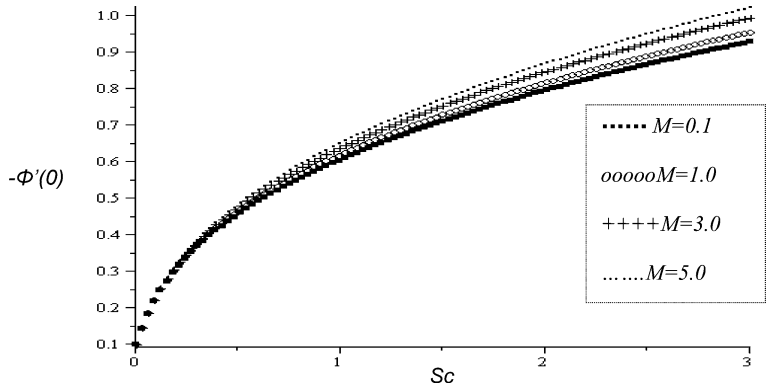

Fig. 21 Local Sherwood number for $G_c = Ra = 0.1$, $K = S = 1$, $Sc = 0.62$, $Pr = 0.72$

4 Conclusions

The problem of mixed convection stagnation flow toward a vertical surface embedded in a highly porous medium with heat and mass in the presence of magnetic field, thermal radiation and internal heat generation is investigated. The governing equations were developed and transformed into a self-similar form. The similarity equations were solved numerically using shooting iteration method together with Runge-Kutta sixth-order integration scheme. From the results of the problem, it was observed that:

1. The velocity profiles overshoot near the plate surface with increasing values of internal heat generation parameter (S), buoyancy parameters (G_T, G_c) and radiation parameter (Ra).
2. The thermal boundary layer thickness increases with increasing radiation parameter (Ra) and internal heat generation parameter (S).
3. The concentration boundary layer thickness decreases with increasing value of Schmidt number (Sc) and solutal Grashof number (G_c).
4. The local skin-friction, local Nusselt number and local Sherwood number increase as magnetic field strength (M) and radiation parameters (Ra) increase.

Acknowledgements The author would like to thank the National Research Foundation of South Africa for their financial support.

References

1. Nield DA, Bejan A (2006) Convection in porous media, 3rd edn. Springer, New York
2. Kumari M, Takhar HS, Nath G (2001) Mixed convection flow over a vertical wedge embedded in a highly porous medium. Heat Mass Transf 37:139–146
3. Chamkha AJ, Quadri MMA (2001) Heat and mass transfer from a permeable cylinder in a porous medium with magnetic field and heat generation/absorption effects. Numer Heat Transf, Part A, Appl 40:387–401
4. Seddeek MA (2002) Effects of magnetic field and variable viscosity on forced non-Darcy flow about a flat plate with variable wall temperature in porous media in the presence of suction and blowing. J Appl Mech Tech Phys 43:13–17
5. Stuart JT (1959) The viscous flow near a stagnation point when the external flow has uniform vorticity. Aerosp Sci Technol 26:124–125
6. Tamada K (1979) Two-dimensional stagnation-point flow impinging obliquely on a plane wall. J Phys Soc Jpn 46:310–311
7. Ali F, Nazar R, Arifin N, Pop I (2011) Effect of Hall current on MHD mixed convection boundary layer flow over a stretched vertical flat plate. Meccanica 46(5):1103–1112
8. Hayat T, Hameed MI, Asghar S, Siddiqui AM (2004) Some steady MHD flows of the second order fluid. Meccanica 39:345–355
9. Ishak A, Nazar R, Pop I (2006) Mixed convection boundary layers in the stagnation-point flow toward a stretching surface. Meccanica 41:509–518
10. Ishak A, Nazar R, Pop I (2008) Mixed convection stagnation point flow of a micropolar fluid towards a stretching sheet. Meccanica 43:411–418
11. Hiemenz K (1911) Die Grenzschicht in einem in den gleichformingen Flussigkeitsstrom eingetauchten gerade Kreiszylinder. Dinglers Polytech J 326:321–410
12. Singh G, Sharma PR, Chamkha AJ (2010) Effect of volumentric heat generation/absorption on mixed convection stagnation point flow on an iso-thermal vertical plate in porous media. Int J Ind Math 2(2):59–71
13. Sparrow EM, Cess RD (1978) Radiation heat transfer. Hemisphere, Washington. Augmented edition
14. Chamkha AJ, Issa C, Khanfer K (2002) Natural convection from an inclined plate embedded in a variable porosity porous medium due to solar radiation. Int J Therm Sci 41:73–81

15. Makinde OD, Ogulu A (2008) The effect of thermal radiation on the heat and mass transfer flow of a variable viscosity fluid past a vertical porous plate permeated by a transverse magnetic field. Chem Eng Commun 195(12):1575–1584
16. Bestman AR, Adiepong SK (1988) Unsteady hydromagnetic free-convection flow with radiative heat transfer in a rotating fluid. Astrophys Space Sci 143:73–80
17. Naroua H, Ram PC, Sambo AS, Takhar HS (1998) Finite-element analysis of natural convection flow in a rotating fluid with radiative heat transfer. J Magnetohydrodyn Plasma Res 7:257–274
18. Ouaf MEM (2005) Exact solution of thermal radiation on MHD flow over a stretching porous sheet. Appl Math Comput 170(2):1117–1125
19. Raptis A, Perdikis C, Leontitsis A (2003) Effects of radiation in an optically thin gray gas flowing past a vertical infinite plate in the presence of a magnetic field. Heat Mass Transf 39:771–773
20. Magyari E, Pantokratoras A (2011) Note on the effect of thermal radiation in the linearized Rosseland approximation on the heat transfer characteristics of various boundary layer flows. Int Commun Heat Mass Transf 38(5):554–556
21. Na TY (1979) Computational methods in engineering boundary value problems. Academic Press, New York